HIFAN 1612

HEAVY ION FUSION SCIENCE VIRTUAL NATIONAL LABORATORY
2nd QUARTER 2010
MILESTONE REPORT
Develop the theory connecting pyrometer and streak camera spectrometer data to the material properties of beam heated targets and compare to the data

by

R.M. More, J. J. Barnard, F.M. Bieniosek, E. Henestroza, S. M. Lidia, P. A. Ni
Lawrence Berkeley National Laboratory (on behalf of U.S. HIFS-VNL)
1 Cyclotron Road, Berkeley, CA 94720

Accelerator Fusion Research Division
Ernest Orlando Lawrence Berkeley National Laboratory
University of California
Berkeley, California 94720

April 2010

This work was supported by the Director, Office of Science, Office of Fusion Energy Sciences, of the U.S. Department of Energy under Contract No. DE-AC02-05CH11231.

HEAVY ION FUSION SCIENCE VIRTUAL NATIONAL LABORATORY

2nd QUARTER 2010

MILESTONE REPORT

Develop the theory connecting pyrometer and streak camera spectrometer data to the material properties of beam heated targets and compare to the data.

R.M. More, J. J. Barnard, F.M. Bieniosek, E. Henestroza, S. M. Lidia, P. A. Ni

1. Executive Summary

This milestone has been accomplished. We have extended the theory that connects pyrometer and streak spectrometer data to material temperature on several fronts and have compared theory to NDCX-I experiments.

For the case of NDCX-I, the data suggests that as the metallic foils are heated they break into droplets (*cf.* HIFS VNL Milestone Report FY 2009 Q4). Evaporation of the metallic surface will occur, but optical emission should be directly observable from the solid or liquid surface of the foil or from droplets. However, the emissivity of hot material may be changed from the cold material and interference effects will alter the spectrum emitted from small droplets. These effects have been incorporated into a theory of emission from droplets.

We have measured emission using streaked spectrometry and together with theory of emission from heated droplets have inferred the temperature of a gold foil heated by the NDCX-I experiment. The intensity measured by the spectrometer is proportional to the emissivity times the blackbody intensity at the temperature of the foil or droplets. Traditionally, a functional form for the emissivity as a function of wavelength (such as a quadratic) is assumed and the three unknown emissivity parameters (for the case of a quadratic) and the temperature are obtained by minimizing the deviations from the fit. In the case of the NDCX-I experiment, two minima were obtained: at 7200 K and 2400 K. The best fit was at 7200 K. However, when the actual measured emissivity of gold was used and when the theoretical corrections for droplet interference effects were made for emission from droplets having radii in the range 0.2 to 2.0 microns, the corrected emissivity was consistent with the 2400 K value, whereas the fit emissivity at 7200 K shows no similarity to the corrected emissivity curves. Further, an estimate of the temperature obtained from beam heating is consistent with the lower value. This exercise proved to be a warning to be skeptical of assuming functional forms when they are unknown, and also represents a first success of the droplet emission theory.

The thermal optical emission from a hot metal surface is polarized (for observation angles that are not normal to the surface). By observing the intensity of both polarizations at two or more observation angles the emissivity can be inferred directly, and the temperature at the surface unambiguously determined. Emission from the s-polarization (where the E-field is parallel to the surface and normal to the wave vector) is generally less intense than emission from the p-polarization (E-field that is normal to the s-polarization E-field and the wave vector.) The emissivity and temperature may be inferred directly without assuming any specific functional form for the emissivity or resorting to published data tables (which usually do not apply when temperatures reach the WDM regime). We have derived the theory of polarized emission from hot metals, and consider an improved method of temperature determination that takes advantage of polarization measurements, which we call polarization pyrometry. Thus far we have successfully applied the theory to electrically heated metallic filaments, and will apply

the theory to beam heated targets when chamber space constraints are removed that will make it feasible to observe the targets at multiple angles.

For the case of experiments on NDCX-II, hydrodynamic expansion on a nanosecond timescale that is comparable to the heating time will result in an expanding fluid, with a strong (but finite) density and temperature gradient. Emission will be observed from positions in the foil near the critical density (where the observation photon frequency is equal to the local plasma frequency). By assuming a brightness temperature equal to the local fluid temperature at the critical frequency, a time history of the emission spectrum from an expanding foil can be synthesized from a hydrodynamic simulation of the target. We find that observations from the ultraviolet to the infrared will allow a probing of the target at different depths, and will allow a test of specific equations of state.

Improved versions of this theory that integrate the electric field along a ray from the interior of the metal to observation point are being constructed to give a more accurate description of the emitted spectrum.

Significance of this milestone: The ability to assess material temperature is crucial for many of the planned experiments on NDCX-I and NDCX-II, such as determination of equation of state in the Warm Dense Matter regime. Completion of this milestone has greatly reduced the uncertainty in the inferred temperature, using the data from a multiple wavelength streak spectrometer or a polarization pyrometer.

2. Results: Connecting spectroscopic data to material properties

Table of Contents

We divide this report into four sections, each describing an advance in understanding the general topic of the theory and interpretation of spectral measurements to infer material properties. The four sections are:

2-I. Streak spectrometer experiments on gold targets on NDCX-I and determination of target temperature

2-II. Theory of emission of light from hot metals: size effect for droplets of liquid metals

2-III. Theory of emission of light from hot metals: polarization effects

2-IV. An estimation of observed intensity versus time from the infrared through the ultraviolet in a hydrodynamically expanding fluid expected on NDCX-II

2-I. Streak spectrometer experiments on gold targets on NDCX-I and determination of target temperature

We describe theory and experiment that demonstrate our improved ability to determine the temperature of warm dense matter using time-resolved measurements of visible light spectra.

The technique we use is an improvement of the widely used method of streaked optical pyrometry (SOP). For our recent experiments on gold foils, irradiated by NDCX-I, optical pyrometry leads to an ambiguous determination of the target temperature. Even more problematic, the best fit to the measurements is given by an unlikely high temperature ~ 7200 K. Separate information about the beam intensity and target heating support a more modest expectation (< 3500 K) for the temperature in the experiments. Here we use handbook data for the optical coefficients n, k of gold and theoretical calculations of emission by droplets of liquid metal to verify that the lower temperature is more likely to be correct.

We also describe theoretical calculations of emission of light by small droplets of molten gold, and find evidence for a strong size effect for droplets at sizes comparable to the wavelength: the emission per unit surface area is larger for small droplets than for bulk flat surfaces or larger droplets having the same temperature. This size effect is caused by wave-interference phenomena. For gold droplets, the size effect enhances short wavelength emission and this tends to raise the apparent temperature of the emitting material. We describe an idea for a polarization pyrometer, which takes enough additional data to provide an unambiguous determination of the temperature even when the high-temperature material properties are not known *a priori*.

2-I-1 Experiments on gold targets

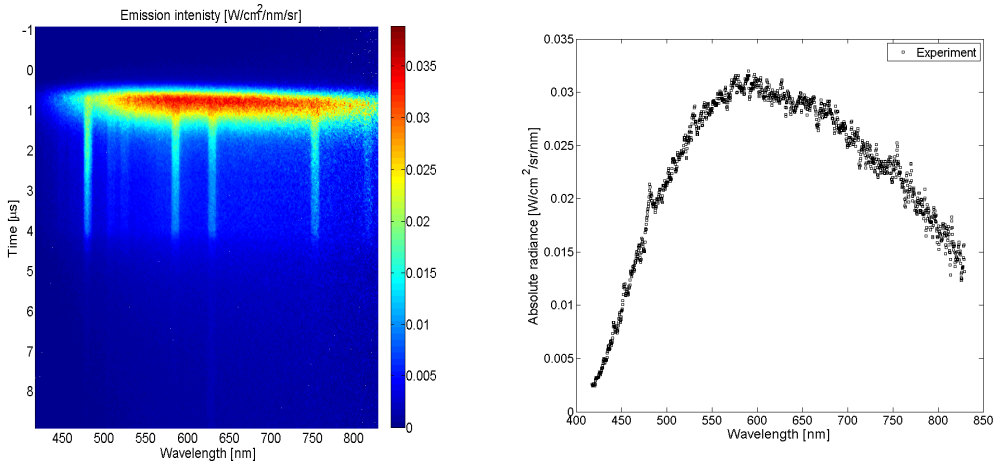

(a) **(b)**

Figure 1. (a) Emission spectrum as a function of time from a beam heated Au target by NDCX-1. **(b)** Emitted intensity versus wavelength at t = 1 μs from spectra in (a).

Gold foils of thickness 0.15 to 0.2 micron were irradiated by 300 keV Potassium +1 ions from NDCX-I. The beam energy flux is determined to be approximately 250 kW/cm^2 at the focal position. Emission spectra were recorded with an approximate time-resolution

of 50 nsec. Figure 1a shows a typical emission spectrum and Figure 1b is a trace through the spectrum at t ~ 1 μsec. We have separate reasons to think the foil has broken into free-standing droplets of liquid metal at this time.

2-I-2 Best-fit to emission data

This data has been analyzed by the usual method of optical pyrometry: the emission spectrum is fit to a blackbody function $B_\nu(T)$ multiplied by an emissivity function $E(\nu)$ which is assumed to be a quadratic function of wavelength $\lambda = c/\nu$ across the visible range. The parameters of the quadratic function are adjusted to optimize the fit. The resulting best fit is shown in Figure 2a and the best-fit emissivity is shown in Figure 2b. The best-fit temperature is 7200 K, which we have reasons to doubt as explained below. However one cannot deny that the fit to experiment is excellent. This fitting procedure is precisely the usual procedure in optical pyrometry and something very similar is used in many laboratories for determining temperatures produced by shock-waves or other warm-dense matter experiments. The weak point of the pyrometry technique is the fact that, over the visible range, a blackbody function with a different temperature (combined with a different emissivity) could fit the data almost equally well. It will have broad implications for WDM science if we can develop a more reliable technique for temperature determination.

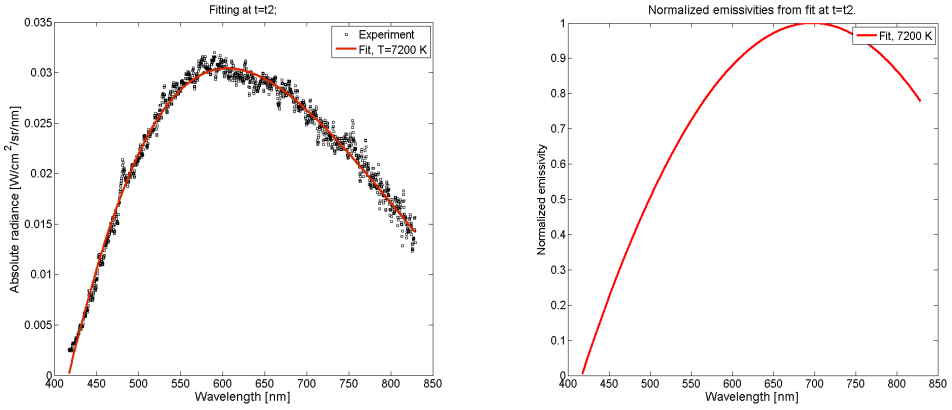

(a) **(b)**

Figure 2. (a) Best fit (with a fitted temperature T = 7200 K) of the spectrometer data (from the data in Fig. 1(b)) using an emissivity assumed to have a quadratic form. **(b)** Inferred best-fit emissivity as function of wavelength.

2-I-3 Target temperature - thermodynamic estimate

From the beam deposition and the specific heat of gold, we obtain a thermodynamic limit on the target temperature. The energy required to heat a 0.2 micron gold foil up to the boiling point (not counting the latent heat of evaporation) is approximately 0.2 Joules/cm^2. To deliver this energy in 1 μsec requires about 200 kW/cm^2. A thick target would be cooled by thermal conduction, but our thin targets do not cool in this way (lateral thermal conduction is negligible on our time-scale). However, the target cools by evaporation at high temperatures.

We estimate the cooling rate at a temperature equal to the normal boiling point, T_B = 3240 K for Au. At this temperature the saturation pressure of gold vapor would be 1 atmosphere.

This corresponds to a gas density of approximately 2.24 10^{18} atoms/cm^3. In equilibrium the evaporation rate would just balance condensation from the saturated vapor, but in vacuum there is little condensation. Assuming a sticking coefficient close to unity, that balance implies an evaporation rate of 3.3 10^{22} atom/cm^2-sec. Each evaporated atom carries away an energy of approximately the latent heat of evaporation, ~ 3.51 eV for gold.

Thus the evaporation cooling heat flux is ~ 18.5 kWatts/cm^2. This should be multiplied by a factor 2 for a thin foil or a factor 4 for spherical droplets (ratio of evaporating surface area to projected area facing the beam). If the ion heating does not deposit more energy than 270 kW/cm^2 (= 200 kW/cm^2 for initial temperature rise + 70 kW/cm^2 for evaporative cooling), the target is expected to reach a temperature lower than the normal boiling point of 3240 K. Based on these numbers, a temperature of 7200 K is clearly impossible with the NDCX-I ion beam.

2-I-4 The second fit to the emission data

The optical pyrometry data is also approximately fit by a different emissivity and a significantly lower temperature. It is quite interesting that this is possible. This second fit is shown in Figure 3a, 3b. The temperature that results is 2400 K, in much better agreement with the thermodynamic temperature limit discussed above.

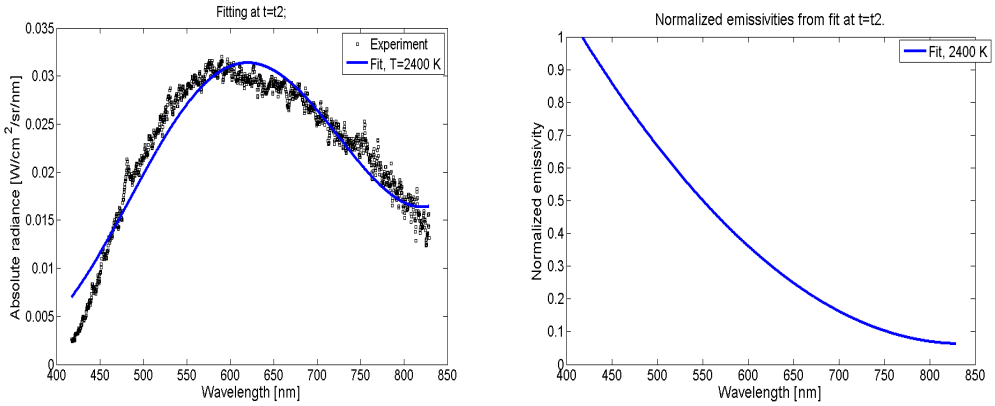

(a) **(b)**

Figure 3. (a) Second fit of the spectrometer data (with a fitted temperature T = 2400 K) (from the data in Fig. 1(b)) using an emissivity assumed to have a quadratic form. **(b)** Inferred fit emissivity as function of wavelength. The parameters derived in figure are also at a minimum in the mean square deviation, but have a larger deviation (worse fit) than those in figure 2. As described in the text, we prefer this fit.

On the basis of the usual optical pyrometry technique, it is difficult to choose between the low (2400 K) and high (7200 K) temperatures (the higher temperature gives a better fit). However a consideration of the optical properties of gold foils and droplets provides a convincing basis to make this choice.

Figure 4 shows a comparison of theoretical emissivity for small (0.2 micron) and large (2 micron) gold droplets. Over the range of visible light wavelengths studied in our experiment, these emissivities are reasonably similar and are much closer to the fitted emissivity in Figure 3b, based on the lower temperature. While the emissivities are calculated from theory using the measured (300 K) optical properties of gold, i.e. using the complex index of refraction $\sqrt{\varepsilon} = n + ik$, published measurements indicate that n, k do not change much at the melting point (see Fig. 4b). Thus the calculation in Figure 4 gives strong support to the lower-temperature fit presented in Figures 3a, 3b.

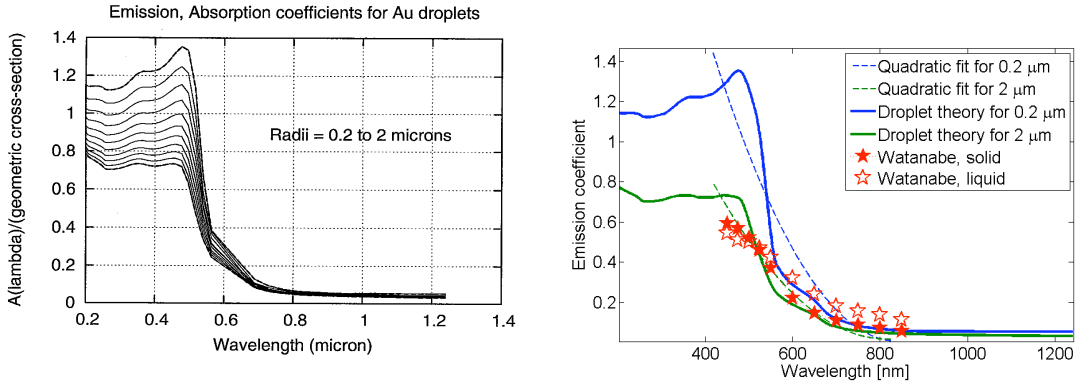

(a) **(b)**

Figure 4. **(a)** Emission/absorption coefficient for gold droplets with radii between 0.2 μ and 2.0 μ (curves shown, starting from the lower curve: radius= 0.2, 0.25, 0.32, 0.40, 0.50, 0.63, 0.80, 1.00, 1.26, 1.59, 2.00 μ) **(b)** Absorption/emission coefficient at 0.2 μ (solid green) and 2.0 μ (solid blue); measured emissivity for solid (300 K) gold (solid red star), and liquid gold (open red star) from Ref. [1] and (dashed) quadratic emissivity that is best fit to the theoretical curves.

The evaporation rate quoted above (3.3 10^{22} atoms/cm^2-sec) would completely evaporate the 0.2 micron foil in 2-10 μsec, consistent with the observed emission (Fig. 1a,b). This calculation is consistent with previous calculations reported in the HIFS VNL FY09 Q4 milestone report.

2-I References

[1] H. Watanabe, M. Susa, H. Fukuyama, K. Nagata, "Phase Dependence (Liquid/Solid) of Normal Spectral Emissivities of Noble Metals at Melting Points, "International Journal of Thermophysics," **24**, 223 (2003).

2-II. Theory of emission of light from hot metals: size effect for droplets of liquid metals

One can see light emitted by glowing hot metals - the kitchen stove, tungsten filaments, or from hot spots on the walls of fusion plasma vessels. It's a disappointment not to find a satisfactory theory for this emission by hot metals in the well-known textbooks of electro-dynamics [1], optics [2] and solid-state physics [3], or even in general textbooks of physics [4].

A metal is a dense plasma having a plasma frequency $\hbar\omega_p \sim 10$ -15 eV. Visible light has $\hbar\omega \sim 2$ eV, so $\hbar\omega << \hbar\omega_p$. A plasma is *overdense* to light of frequency ω if $\omega < \omega_p$ and $\mathrm{Re}[\,\varepsilon(\omega)\,] < 0$, where $\varepsilon(\omega)$ is the frequency-dependent dielectric function. Light reflects from a smooth metal surface and only an evanescent wave penetrates over a skin depth $\delta \sim c/\omega_p \sim 10$ nm. Electrons deep in the metal emit much less light than electrons near the surface even if they have the same local density-temperature conditions; emission is suppressed because the electrons only connect to the exponential tail $\sim \exp(-x/\delta)$ of the light waves.

Metals such as W, Au, Al and Pt have been used for NDCX-I experiments. The cold-matter optical properties are summarized by a dielectric function $\varepsilon(\omega)$ [5]. When the metals are heated to Warm Dense Matter (WDM) temperatures ~ 1 eV, it will be necessary to guess $\varepsilon(\omega)$ in order to compare to experiments. In order to do that comparison one needs equations that apply for an arbitrary dielectric function $\varepsilon(\omega)$. At high temperatures metals evaporate and expand. For very hot metal, the expansion is a release or rarefaction flow; hydrodynamic calculations predict the ρ, T profile [6]. The metal cools as it expands, so the outer layers are cooler than the interior.

In WDM experiments, the temperature has strong gradients. WDM density and temperature may vary over distances much less than the wavelength of light. In this case the emission cannot be calculated from absorption by Kirchhoff's law, and requires a microscopic emission theory.

The equation of radiative transfer gives the radiation energy flow as an integral along light ray paths [6]. This equation applies when the spatial gradients are small over a photon mean free path and very small over the wavelength of light. Neither condition is satisfied for most WDM experiments. In addition, light rays are undefined in overdense plasma because the index of refraction $\sqrt{\varepsilon} = n + ik$ is a complex number. For these reasons emission of visible light by overdense metals cannot be described by the usual radiative transfer theory.

For a more satisfactory description, the emitted radiation is given by an integral over the sources, which are fluctuating microscopic currents inside the metal. The theory naturally invokes the Weiner-Kinchin theorem for stationary random processes and the Kubo formula (fluctuation-dissipation theorem). With these equations the emission is

given by an integral over the local dielectric function, as described in section 2-III-2 below.

2-II-1 Emission by small droplets of liquid metal

Accelerator-heated WDM experiments on NDCX-I rapidly heat a submicron-thick foil to several thousand K. The foil appears to break into small droplets of liquid metal and time-resolved emission spectra are measured. We would like to extract information from those spectra to decide the temperature of the hot material and, if possible, the size of the droplets. At the conditions of the experiments the metal inside the droplets probably has uniform density and temperature.

In this case Kirchhoff's law applies and we can calculate the emission from the absorption cross-section A(ω). The total power emitted into 4π steradians is

$$\frac{dE}{dt} = \int \frac{(\hbar\omega)^3}{\pi^2\hbar^3c^2}\frac{A(\hbar\omega)}{(e^{\hbar\omega/kT}-1)}d\hbar\omega$$

A(ħω) is the absorption cross-section for a plane wave approaching the droplet. We calculate A(ħω) from Mie theory of light scattering by a small droplet [1, 2, 7].

The electromagnetic fields are represented as a series of vector spherical harmonic functions. Inside the droplet there is an evanescent wave, which has a complex wave-number

$$K = (\omega/c)\ \sqrt{\varepsilon}$$

To evaluate the formulas we need Bessel functions $j_\ell(Kr)$ for complex wave-number K and for large index ℓ (up to 200). To generate these functions we use a recursion formula *iterating down* ($\ell \rightarrow \ell$-1) for the Bessel function j_ℓ and *iterating up* ($\ell \rightarrow \ell$+1) for the Neumann function n_ℓ. A Bessel-function theorem helps evaluate the volume-integral of the Joule heating to calculate the absorption. We evaluate the formulas using measured dielectric functions [5], which are valid for room-temperature material.

A useful check of the computer code is the comparison to an analytic formula (Eq. 93-4 of reference [4]) valid for droplets that are small compared to the wavelength. Our code agrees accurately with this formula for $R \ll \lambda$.

A comparison to geometrical optics agrees to a few percent for large spheres ($R \gg \lambda$). The droplet calculations are only relevant in a limited temperature range between melting and boiling temperatures. At higher temperatures, evaporation or rarefaction flow will rapidly produce a nonuniform density-temperature profile and we must calculate the emission without using detailed balance.

2-II References

[1] J. D. Jackson, *Classical Electrodynamics*, 3rd Ed., J. Wiley, Hoboken, NJ (1999).
[2] M. Born and E. Wolf, *Principles of Optics*, 5th Ed., Pergamon Press, Oxford (1975).
[3] C. Kittel, *Introduction to Solid-State Physics*, 3rd Ed., Wiley, NY (1967); F. Seitz,

Modern Theory of Solids, Dover, NY (1987); W. Jones and N. H. March, *Theoretical Solid State Physics*, Dover, NY (1985).
[4] E. Landau and I. M. Lifshitz, *Electrodynamics of Continuous Media*, 2nd Ed., Pergamon Press, Oxford, (1984). (See section 93, eq. 93-4.)
[5] E. Palik, *Handbook of Optical Constants of Solids*, Academic Press (1985).
[6] Ya. Zel'dovich & Yu. Raizer, *Physics of Shock Waves and High-Temperature Hydrodynamic Phenomena*, Dover, (2002).
[7] H. C. Van de Hulst, *Light Scattering by Small Particles*, Dover Publications, New York, 1981.

2-III. Theory of emission of light from hot metals: polarization effects

2-III-1 Emission by a uniform hot metal

For a hot metal layer in which the temperature is uniform we can calculate the emission from the absorption coefficient using Kirchhoff's law. This special case gives a useful test for the general theory of emission.

To calculate the absorption during reflection from a flat metal surface, one solves the Maxwell eqs. for the classical **E**, **B** fields. The energy flow into the material is S_x = x-component of the Poynting vector, where x is the direction into the material (the surface is the yz plane). The energy absorption is

$$\frac{dS_x}{dx} = -\mathrm{Re}[\ \sigma(\omega)\ ]\left\langle \left|\vec{E}(x)\right|^2 \right\rangle$$

which is equal to the local Joule heating. To evaluate this one needs the high-frequency conductivity $\sigma(\omega)$, related to the dielectric function by

$$\varepsilon(\omega) = 1 + 4\pi i\sigma(\omega)/\omega$$

so

$$\mathrm{Re}[\ \sigma(\omega)\ ] = \omega\ \mathrm{Im}\ [\ \varepsilon(\omega)\ ]/4\pi$$

In all cases, the theory predicts that p-polarized absorption is larger than s-polarized absorption

$$A_p > A_s$$

The s- and p-polarized absorptions differ, in part, because p-polarized light induces a surface-charge density.

A technique of ultra-short pulse pump-probe ellipsometry can give quantitative information about laser-heated materials with subpicosecond time resolution [1]. The absorption theory is well-tested by laser experiments and measurements on cold matter. The absorption coefficients A_s, A_p are readily measured by short-pulse laser experiments.

If the metal has constant temperature and density, the absorption coefficients are given by the Fresnel formulas, evaluated with the optical constants n and k determined by $\varepsilon(\omega) = (n+ik)^2$. However the Fresnel formulas fail as soon as the metal surface begins to expand [2] or when there is a significant temperature gradient in the surface skin depth region. In that case a more elaborate emission theory is needed.

2-III-2 Emission by a nonuniform metal surface

A general theory of emission is more difficult. We examine the absorption and emission for a normal mode of the radiation field characterized by a free-space wave-vector (k_x, k_y, k_z). Light absorption is coherent and stimulated emission is a coherent reduction of the absorption, but for the materials considered here the spontaneous emission is incoherent.

Electric and magnetic fields made by the sources are linearly related to the sources,

$$\mathbf{E} = \mathbf{G}_E \circ \mathbf{j} \quad \text{and} \quad \mathbf{B} = \mathbf{G}_B \circ \mathbf{j}$$

where the Green's functions $\mathbf{G}_E$ and $\mathbf{G}_B$ depend on polarization (selected by the direction of the current fluctuations $\mathbf{j}$) and the circle ("o") represents a convolution integral. The Green's functions include the coherent response of the medium (overdense "refraction", absorption, stimulated emission) as described by the dielectric function $\varepsilon(\omega)$. The G's are constructed as products of matrices for layers of target material; they decrease like $\exp(-\mathrm{Re}[\gamma]x)$. Here γ is the x-component of the wave-vector inside the metal,

$$\gamma^2 = (\omega^2/c^2)[\sin^2\theta - \varepsilon(\omega)]$$

Of course the electric field oscillates rapidly and its time-average is zero. We examine a quadratic quantity, the Poynting vector

$$\mathbf{S} = c(\mathbf{E}\mathrm{X}\mathbf{B})/4\pi$$

$\mathbf{S}$ is a sum over the incoherent sources, which are microscopic currents in the material. The emission can be written symbolically:

$$\mathbf{S} \sim (c/4\pi) \int \mathbf{G}_E \,\mathrm{X}\, \mathbf{G}_B \circ \langle \mathbf{j} \circ \mathbf{j} \rangle \, dx$$

Here $\langle \mathbf{j} \circ \mathbf{j} \rangle$ is the current fluctuation, related to the current-current autocorrelation function by the Weiner-Kinchin theorem. The Kubo relation connects this quantity to the real part of the AC electrical conductivity $\mathrm{Re}[\sigma(\omega)]$ which is in turn proportional to $\mathrm{Im}[\varepsilon(\omega)]$, the imaginary part of the dielectric function.

The difficult part of this calculation is the calculation of the Green's functions, but there is a simple and convincing way to check the calculation. For a uniform metal plate (having constant composition, density and temperature) the emitted spectrum exactly equals the absorption from a blackbody spectrum having the same temperature, i.e., the power emitted from a given layer into a given solid angle in a given frequency range

equals the power absorbed in the same layer from the same solid angle at the same frequencies.

The equations predict a phenomenon of *overdense radiation transport* which we have not seen discussed in the previous scientific literature. When a source at depth x_S makes electric and magnetic fields, some of the energy of these fields is absorbed in a second layer at depth x_T. The Green's functions describe that absorption through the Im [ε] in the wave-equation. However, if the material temperature is uniform (homogeneous), the second region at x_T also emits radiation and some of that penetrates back to x_S and is absorbed there. These two absorptions are exactly equal if the temperatures $T(x_S)$ and $T(x_T)$ are equal, and that is a powerful consistency check for the theory (Onsager symmetry). If the two temperatures are not equal, there is a net heat conduction from hot to cold. Because the overdense radiation field typically does not have a large energy-density (compared to the material energy-density) this overdense transport is not a strong correction to the normal electron heat conduction, but it is a powerful check of our calculations to find that it obeys the principle of detailed balance.

The calculations described here predict that emission from hot metals (having smooth and clean surfaces) should be strongly p-polarized, when seen from a sufficient angle from the normal.

2-III-3 Polarization and pyrometry

Polarized emission from metals was observed many years ago (Millikan [3]), but apparently is not well known: it is not even mentioned in several modern textbooks [4]. Probably magnetic fusion machines are filled with polarized visible light emitted by hot metal on the limiter, divertor, etc.

In the National Institute for Fusion Science, our collaborators (M. Goto et al.) recently measured polarized emission for electron-beam heated foils of W metal. The experiments observed polarization resolved spectra of radiation from the tungsten surface which was heated by an electron beam. The viewing angle to the surface was 75 degree from normal to the surface. One component is polarized parallel (II) to the surface and the other (⊥) is perpendicular to it. The temperature was estimated from the spectra. The radiation is strongly polarized. The experiments study the polarization at different temperatures and some temperature-dependence of the polarization was observed at the highest temperatures. In the Lawrence Berkeley National Laboratory and the University of Electro-Communication, H. Yoneda and P. Ni have observed polarized emission from electrically heated strips of several metals.

Optical pyrometry is a well-known way to determine temperature from emitted light. The optical pyrometer has limited time-response and temperature sensitivity because it must collect enough photons to obtain accurate data. The usual optical pyrometer is an imperfect thermometer for another reason: one measures the emitted intensity $I(\omega_j)$ at N wavelengths, but there are almost always N+1 unknowns: the N emissivities $E(\omega_j)$ *and*

the surface temperature T. One can only extract a temperature by making some assumption about the frequency-dependence of the surface emissivity E(ω).

For this reason we are exploring the possibility of a *polarization pyrometer*, which will measure emission of the two polarizations at several angles. In this way one can collect enough data to unfold the unknown dielectric function and the unknown temperature. This is especially important for WDM where we do not *a priori* know the emissivity E(ω) or dielectric function ε(ω).

2-III-4 Summary and conclusions

1.) We have studied the general theory of emission of radiation by hot dense matter.
2.) Our computer codes predict light emission using material descriptions obtained from hydrodynamic codes.
3.) We predict that light emitted from a smooth clean hot metal surface is predominantly p-polarized.
4.) The codes provide a tool for improving the interpretation of pyrometry measurements of emission and finding a more convincing determination of WDM plasma temperatures from pyrometry measurements.

2-III References

[1] H. Yoneda, H. Morikami, K. Ueda and R. More, Physical Review Letters **91**, 075004 (2003); H. Yoneda, H. Morikomi, K.-I. Ueda and R. More, J. Plasma Fusion Res. 79, 449 (2003).
[2] H. Morikami, H. Yoneda, K.-I. Ueda and R. M. More, Phys. Rev. **E70**, 035401 (2004).
[3] R. A. Millikan, Phys. Rev. **3**, 81 (1895); Phys. Rev. **3**, 177 (1895); see also A. G. Worthing, J. Opt. Soc. Am. & RSI **13**, 635 (1926).
[4] M. Born and E. Wolf, *Principles of Optics*, 5th Ed., Pergamon Press, Oxford (1975).
[5] A. Sommerfeld, *Optics*, Academic Press, NY, (1954).

2-IV. Estimation of observed intensity versus time from the infrared through the ultraviolet in expanding material from NDCX-II targets

2-IV-1 Introduction

Ion beams have a number of advantages for heating materials to the Warm Dense Matter (WDM) state [1 - 4]. Included among these are capabilities for spatially uniform and volumetric energy deposition over relatively large and diagnosable material volumes. The Neutralized Drift Compression Experiment (NDCX II) is now being constructed at Lawrence Berkeley National Laboratory to study Warm Dense Matter questions and to investigate target-beam coupling relevant to heavy-ion driven inertial fusion energy. NDCX II is the successor to NDCX I [5]. The physics design of the NDCX II accelerator is described elsewhere [6]. In section 2-IV-2, we review the target configurations considered for NDCX II. In section 2-IV-3, we give an example of a particular simulation

of a solid Aluminum foil target. In section 2-IV-4, we examine the expected temperature and velocity at the critical surface that are related to measurements of an instantaneously heated ideal gas. In sections 2-IV-5 and 2-IV-6 we examine predictions of the same measurements derived from simulations of a more realistic equation of state, heated over a finite pulse duration with realistic ion deposition by a beam. Finally, in section 7 we summarize our results.

2-IV-2 Target configurations for NDCX II

A number of target configurations have been considered for NDCX II. These include spherical [7] and cylindrical bubbles [8] (to create enhanced regions of higher pressure and temperature) and planar solid and planar foam [9] targets. Pulse formats include single pulses of fixed ion energy (but with an energy spread at the target) for WDM studies, and double pulses with varied energy (or single pulses with ion energy that changes over the pulse) to investigate ion-coupling efficiency[10]. Recent heavy ion driven "direct drive" target simulations for inertial fusion energy have shown promisingly high fusion gain [11], by increasing the range over the course of the pulse. This increasing range can be accomplished by increasing the ion energy over the course of the pulse. Experiments that demonstrate increased coupling efficiency by increasing the range over the course of the pulse have been simulated[10]. In this report, however, we focus on the WDM mission for NDCX II.

2-IV-3 Simulation of beam-heated solid aluminum target

As described in section 2-IV-2, NDCX II is being designed to heat both solid and porous planar metallic foils, among other options. For the simulations described in this paper we used the radiation hydrodynamics code HYDRA [12]. We assumed the target material was a 3.5 μm thick solid Aluminum, and that the equation of state was either QEOS [13] or LEOS (see fig. 1), both of which are available to the HYDRA code. The ion intensity varied with time as a parabola of full width duration 1 ns. The ion beam used was a 2.8 MeV Li^+ beam and the simulation used HYDRA's Bethe-Bloch ion deposition algorithm. The intensity was adjusted to yield approximately 20 kJ/g integrated over the pulse, significantly higher than the NDCX-I experiments described above. The HYDRA simulations were 2D with an assumed 0.5 mm beam radius; the results here simply describe the 1D evolution of the target along the longitudinal axis (parallel to the beam direction). Figure 2 describes the evolution of the density, temperature, velocity, and charge state Z* of the target during the 1 ns of heating of the pulse.

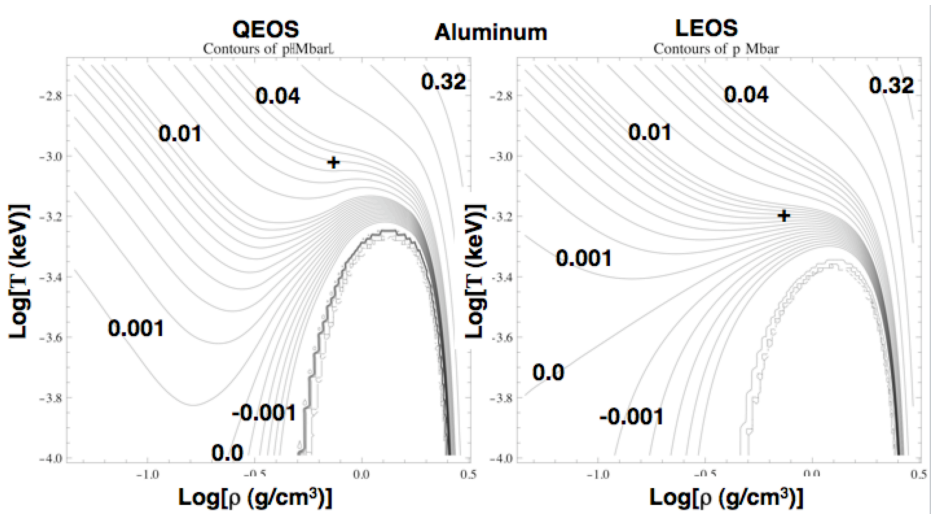

Figure 1. Isobars of pressure (in MBar) as a function of temperature and density for two different equations of state used by the HYDRA code (QEOS and LEOS). Crosses indicate location of critical point.

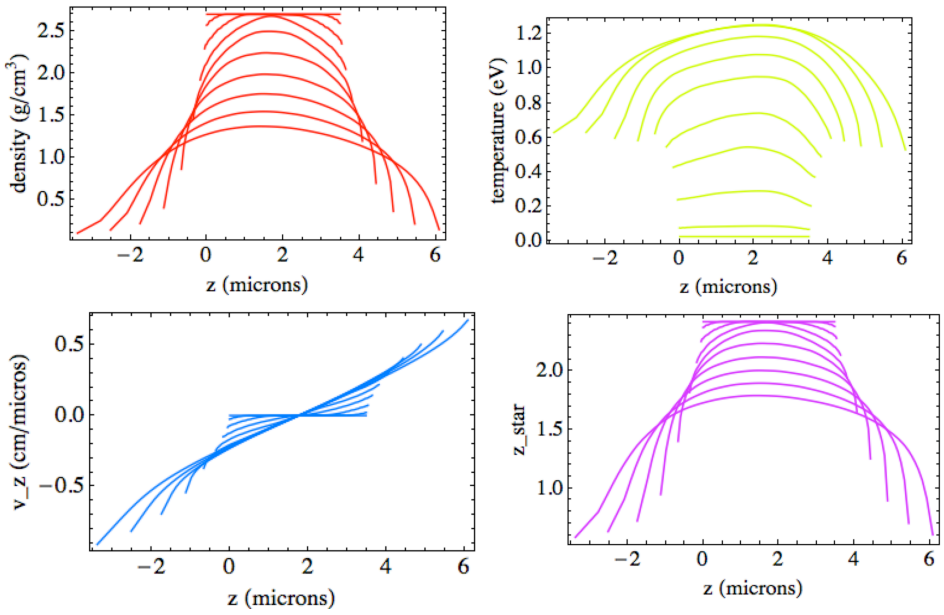

Figure 2. Longitudinal variation of target at radial center (r=0) for ten different times equally spaced between 0 and 1 ns. Ion beam heating ends at 1 ns. Target initially lies between 0 and 3.5 microns. Upper left: Density vs. longitudinal distance z; Upper right: Temperature kT vs. z. Lower left: Longitudinal velocity v_z vs. z; Lower right: Effective charge state of target Z^* vs. z.

2-IV-4 Instantaneously heated, idealized slab

As a way of qualitatively understanding foil expansion we may look at the analytic solution to the idealized problem of a foil that is instantaneously heated, has an ideal gas equation of state and expands isentropically [14, 15]. In this case, a rarefaction wave propagates inward at the initial sound speed c_s of the foil (calculated using the initial

temperature after instantaneously heating but before any expansion). The front of the relaxation wave propagates outward at $2c_s/(\gamma\text{-}1)$, equal to $3c_s$ for a perfect monatomic gas, for which the ratio of specific heats $\gamma=5/3$. It is useful to calculate the critical frequency as a function of the longitudinal position. For a particular emission frequency ν, light propagation becomes evanescent when the frequency falls below the critical frequency ν_{crit} in the medium (equal to the angular plasma frequency ω_p in the medium divided by 2π). This relation can be written,

$$h\nu_{crit} = h\omega_p/2\pi = 28 \text{ eV } \sqrt{\rho(\text{g/cm}^3)Z^*/A_{\text{target}}} \qquad (1)$$

Here Z^* is the effective charge state of the medium, ρ is the mass density and A_{target} is the atomic mass number of the target. If we further assume in this example that Z* is fixed, it is apparent that lines of constant critical frequency are coincident with lines of constant density. Further, the assumption of instantaneous heating implies that all fluid elements have the same entropy equal to their initial value. For such a fluid, the pressure P can be written as a function only of the density ρ, $P = K\rho^\gamma$ and it follows that $T \sim \rho^{\gamma-1}$, and so lines of constant temperature are coincident with lines of constant density. If we model the emission from such a slab, by assuming emission at the blackbody intensity from the location of the critical frequency, we can get a qualitative picture of the emission evolution as a function of time. If at a given frequency, the critical frequency for all parts of the slab lies below the observation frequency, we assume that the observed intensity will be that at the maximum (central) temperature in the slab. (In fact, an integration that includes contributions from all portions of the slab is appropriate and in order. Here we simply assume the steep temperature dependence on emission will dominate the emergent spectra.) Figure 3 shows the trajectory in the z, t plane of the constant density surface. It is clear that for sufficiently low observation frequencies, the point of emission will first propagate outward and then plunge toward the axis. During this time, the brightness temperature will be constant (since the temperature will be constant along the density contour), and a "plateau" in the emission will be observed.) The length of the plateau will be dependent on the frequency of the emission. From the approximate analytic formula in ref. [12] we find that the central density ρ_{center} evolves with time t as:

$$\frac{\rho_{center}}{\rho_0} = \frac{3}{2}\left(1 - \frac{1}{\tau^{1/2}} + \frac{1}{3\tau} - \frac{1}{3\tau^{3/2}}\right)/(3\tau - 4\tau^{1/2} + 1) \qquad (\tau > 1) \qquad (2)$$

Here we have again assumed a $\gamma=5/3$ perfect gas, $\tau\ (= c_s\ t/L)$ is the time measured in hydrodynamic timescales L/c_s, and the formula is valid for $\tau > 1$. (For $\tau < 1$, $\rho_{\text{center}} = \rho_0$). For $\tau >> 1$, eq.[2] reduces to $\rho_{center}/\rho_0 \approx 1/(2\tau)$. This implies that the duration Δt of the constant density contour varies according to density as $\Delta t \approx L\rho_0/(2\rho c_s)$, and since $\nu_{crit} \sim (\rho Z^*)^{1/2}$ then $\Delta t \sim L\,\nu_{crit0}^2 Z^{*2} / (2\,L\,\nu_{crit}^2\, Z_0^{*2}\, c_s)$, and the condition $\tau >> 1$, requires that $\nu_{crit0} Z_0^* / (\nu_{crit} Z^*) >> 1$. Here subscript 0 indicates a quantity right after the instantaneous heating (t=0). If Z* is constant, then the low frequency observers of emission from the critical surface will see constant emission for a timescale that is longer than the hydrodynamic timescale by a factor $(\nu_{crit0}/\nu_{crit})^2$. The temperature of material at the critical frequency is given by $T/T_0 = (\rho/\rho_0)^{2/3} = (\nu_{crit} Z_0^* / [\nu_{crit0} Z^*])^{4/3}$.

As an example, if the initial central critical frequency (times Planck's constant) is 14 eV, and the initial central temperature is 2 eV, an observer of an infrared photon energy of 0.8

eV would observe that the critical surface would have (assuming $Z_0^* / Z^*=1$) a temperature of 0.04 eV, and it would remain at a constant intensity for 306 hydrodynamic times L/c_s. In more realistic situations, as the density is lowered, Z* is lowered, so that the temperature is not as low, and the time duration is not as long.

As can be seen from figure 3, initially the velocity contours overlie the density contours so that for a time the velocity of the critical surface is constant. However, after the time at which the density contour plunges towards the axis z/L =1 (at the boundary between the so-called simple and non-simple wave solution), the density contours are crossing the velocity contours, so that during this "plunge" the velocity of the critical surface tends towards zero, the value it reaches when it reaches the center of the target (z/L =1). During the initial evolution, under the same assumptions as above, the velocity of the critical surface satisfies: $v= 3\ c_s\ ((\nu_{crit} Z_0^* / [\ \nu_{crit0} Z^*])^{2/3}-1)$. Using the same parameters as the example above the velocity of the 0.8 eV (IR) surface would have maximum magnitude 2.55 c_s and then tend to zero at 306 L/c_s (at the end of the plateau in T).

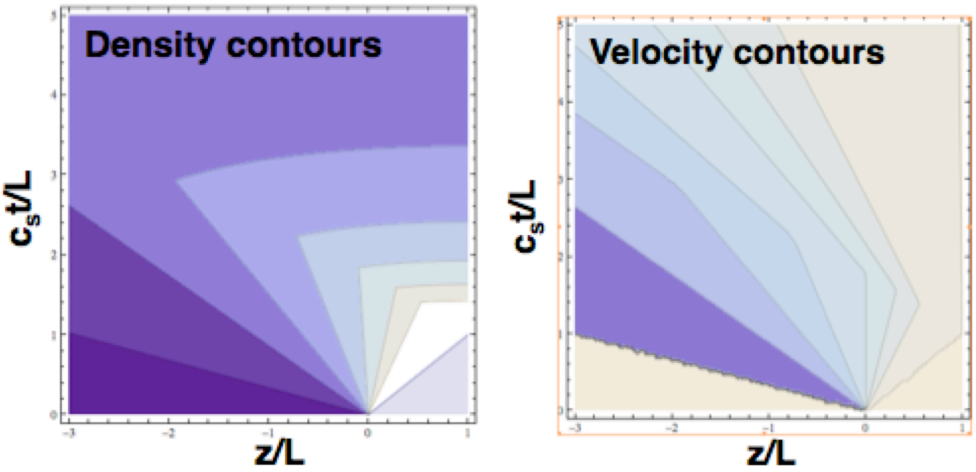

Figure 3. Density (left) and velocity (right) contours as a function of longitudinal position and time. Here the instantaneously heated foil is located between z=0 and z=2L, with only the left half-plane shown. The right half plane is a mirror reflection. The quantity c_s is the initial sound speed (after the instantaneous heating occurs at t=0).

2-IV-5 Predicted brightness temperature evolution for beam heated Aluminum target

For the target that is heated in a finite pulse duration, with finite non-uniformity, with a non-ideal gas equation of state, and an evolving Z*, the evolution will differ from that described in section 2-IV-4. As a way of testing the ability of pyrometer measurements [15] to discriminate equations of state in an actual experiment, we estimated the temperature as a function of time as measured by a pyrometer at three widely separated wavelengths, using the ion pulse parameters and two EOS's described in section 2-IV-3. For the brightness temperature, we again assume the following model for the brightness temperature T_b:

$$T_b = \begin{cases} T_{\max} & \text{if} \quad \nu > \nu_{crit\,\max} \\ T(\nu_{crit}) & \text{if} \quad \nu_{crit\,\max} > \nu > \nu_{crit\,\min} \\ 0 & \text{if} \quad \nu_{crit\,\min} > \nu \end{cases} \qquad (3)$$

Here T_{max} is the maximum material temperature within the foil (generally found at the foil center), $\nu_{critmax}$ is the maximum critical frequency in the foil (also usually at the center) and $\nu_{critmin}$ is the minimum critical frequency in the simulation (usually at the outermost zone, numerically limited by the finite density of the lagrangian fluid element). The results for the NDCX II simulations are found in figs. 4 and 5.

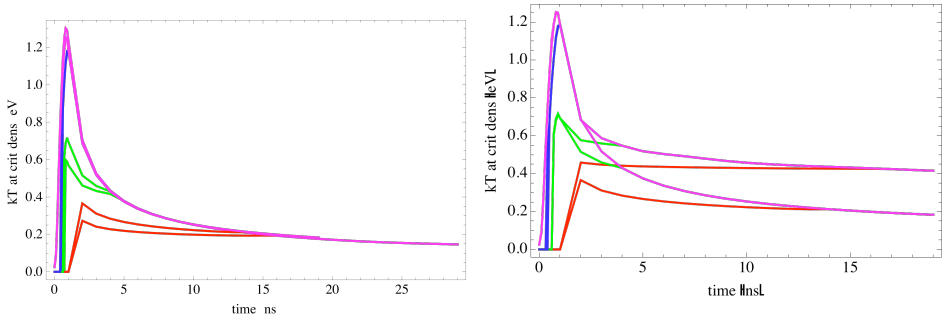

Figure 4. Left: Evolution of brightness temperature (defined in eq. 3) for three observation photon energies (red: 1500 nm; green 450 nm, and blue: 150 nm) and two equations of state (upper: LEOS; lower: QEOS). Both EOS are without Maxwell construction. The magenta curve is the evolution of T_{max}. Right: Same as left figure, except that the upper curves are LEOS without Maxwell construction, and the lower curves are with the Maxwell construction.

2-IV-6 Predicted velocity evolution for beam heated Aluminum target

We may similarly calculate the velocity that would be inferred by a reflected laser pulse if the reflection occurs predominantly at the critical frequency. These results are shown in figure 4.

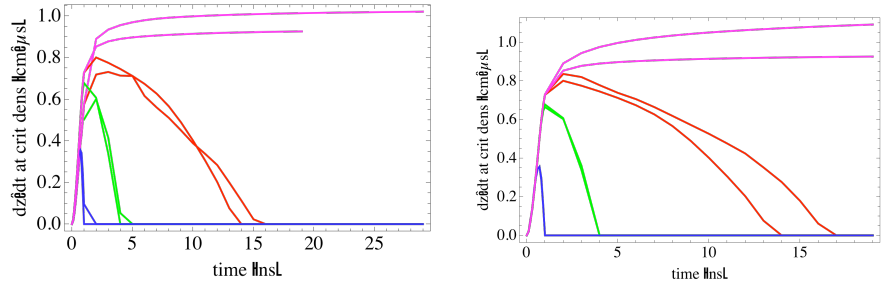

Figure 4. Left: Evolution of velocity at the critical density for three observation photon energies (red: 1500 nm; green 450 nm, and blue: 150 nm) and two equations of state (upper: LEOS; lower: QEOS). Both EOS are without Maxwell construction. The magenta curve is the evolution of v_{max}, the velocity of the outermost zone. Right: Same as left figure, except that the upper curves are LEOS without Maxwell construction, and the lower curves are with the Maxwell construction.

2-IV-7 Discussion and conclusion

It is evident from figures 3 and 4 that widely spaced wavelength pyrometry measurements of expanding foils will differ at the 15 to 25% level, between the two equations of state (QEOS and LEOS) that have differences as shown in Fig. 1. The qualitative results of section 2-IV-4 are confirmed. Namely, the brightness temperature is lower at lower frequencies and the pulse duration is longer. It is also worth noting that the choice of whether to use the Maxwell construction in hydrodynamic simulations also makes significant and measurable differences to predicted pyrometry measurements, particularly in the IR for these parameters. The choice of which construction to use is non-trivial. Maxwell construction implies equilibrium has occurred over the length scale of the simulation zone, even in the dynamically changing situation of a rapidly expanding foil. Simulation without the Maxwell construction implies that droplets and bubbles are well resolved, which is unlikely to be true at all scales [16].

For the velocity measurements, the differences between EOS (and between simulations with and without Maxwell construction) are most clearly seen in the longer wavelength results; the differences are on the 10% level for the two candidate EOS's.

We should point out that these calculations have neglected any absorption through the medium and any differences between the propagation of the two polarization states, and so are really only a first look at the ability of NDCX II to clarify EOS questions. We have also used a solid target as the most rigorous test, as the hydrodynamic time scale for this case is the shortest relative to the pulse duration of NDCX II. Including these additional physics and a wide range of materials is currently under study by the authors. Finally we should note that these calculations can also be applied to (and were partially motivated by) laser heated targets if there is initial temperature equilibration followed by hydrodynamic expansion [17].

2-IV References

[1] B.G. Logan, et al., "Heavy ion fusion science research for high energy density physics and fusion applications," IFSA 2007, Journal of Physics, Conference Series **112** (2008) 032029.

[2] N.A. Tahir, P. Spiller, S. Udrea, O.D. Cortazar, C. Deutsch, V.E. Fortov, V. Gryaznov, D.H.H. Hoffmann, I.V. Lomonosov, P. Ni, A.R. Piriz, A. Shutov, M. Temporal, D. Varentsov," Studies of equation of state properties of high-energy densitymatter using intense heavy ion beams at the future FAIR facility: The HEDgeHOB collaboration," Nuclear Instruments and Methods in Physics Research B **245** (2006) 85–93.

[3] J.J. Barnard, et al., "Accelerator and ion beam tradeoffs for studies of warm dense matter," Proc. 2005 Particle Accelerator Conference, p. 2568 (2005).

[4] F.M. Bieniosek, E. Henestroza, M. Leitner, B.G. Logan, R.M. More, P.K. Roy, P. Ni, P.A. Seidl, W.L. Waldron, J.J. Barnard, "High energy density physics experiments with intense heavy ion beams," Nucl. Instrum. Meth. A 606 (2009) 146-151.

[5] P.A. Seidl, A. Anders, F.M. Bieniosek, J.J. Barnard, J. Calanog, A.X. Chen, R.H. Cohen, J.E. Coleman M. Dorf, E.P. Gilson, D. P. Grote, J.Y. Jung, M. Leitner, S.M. Lidia, B.G. Logan, P. Ni, P.K. Roy, K. van den Bogert, W.L. Waldron, D.R. Welch,

"Progress in beam focusing and compression for warm-dense-matter experiments," Nucl. Instrum. Meth. A **606** (2009) 75-82.
[6] A. Friedman *et al*., Nucl. Instr. and Meth. A **606**, 6 (2009).
[7] S. F. Ng, J. J. Barnard, P. T. Leung, B.G. Logan, and S. S. Yu, in preparation (2010).
[8] J. J. Barnard, J. Armijo, D. S. Bailey, A. Friedman, F. M. Bieniosek, E. Henestroza, I. Kaganovich, P. T. Leung, B. G. Logan, M.M. Marinak, R. M. More, S. F. Ng, G. E. Penn, L. J. Perkins, S. Veitzer, J. S. Wurtele, S. S. Yu, A. B. Zylstra, "Ion beam heated target simulations for warm dense matter physics and inertial fusion energy," Nuclear Instruments and Methods in Physics Research A, **606**, 134-138, (2009)
[9] A. B. Zylstra, J.J. Barnard, and R. M. More, High Energy Density Physics (2010), in press.
[10] S. F. Ng, S. Veitzer, J. J. Barnard, P. T. Leung, S. S. Yu, in preparation (2010).
[11] B. G. Logan, L. J. Perkins, and J. J. Barnard, Phys. Plasmas **15**, 072701 (2008).
[12] J. J. Barnard, J. Armijo, R. M. More, A. Friedman, I. Kaganovich, B. G. Logan, M. M. Marinak, G. E. Penn, A. B. Sefkow, P. Santhanam, P. Stoltz, S. Veitzer, J. S. Wurtele, "Theory and Simulation of Warm Dense Matter Targets," Nuclear Instruments and Methods in Physics Research A, **577** (2007) 275-283.
[13] R. More, K.H. Warren, D.A. Young, G. B. Zimmerman, "A new quotidian equation of state for hot dense matter", Phys. Fluids, **31**, 3062 (1988).
[14] L.D. Landau and E.M. Lifshitz, "Fluid Mechanics," Pergamon Press (chapter 10) (1959).
[15] P.A. Ni, M.I. Kulish, V. Mintsev, D.N. Nikolaev, V.Ya. Ternovoi, D.H.H. Hoffmann, S. Udrea, A. Hug, N.A. Tahir, D. Varentsov, "Fast six-channel pyrometer for warm-dense-matter experiments with intense heavy-ion beams", Laser and Particle Beams, December 2008.
[16] J. Armijo and J.J. Barnard, in preparation (2010).
[17] P. A. Ni, F. M. Bieniosek, M. Leitner, C. Weber, W. L. Waldron, "Testing of optical diagnostics for ion-beam driven WDM experiments on NDCX-I," Nuclear Instruments and Methods in Physics Research A, **606**, (2009), 169-171.